The molecular signatures of compatible and incompatible pollination

Authors: Chie Kodera[1*], Jérémy Just[1], Martine Da Rocha[2], Antoine Larrieu[1,+], Lucie Riglet[1], Jonathan Legrand[1,3], Frédérique Rozier[1], Thierry Gaude[1], Isabelle Fobis-Loisy[1*,]

[1] Laboratoire Reproduction et Développement des Plantes, Univ Lyon, ENS de Lyon, UCB Lyon 1, CNRS, INRA, Lyon, France

[2]INRA, Université Côte d'Azur, INRA, CNRS, ISA 400 route des Chappes BP 167, 06903 Sophia Antipolis Cedex, France

[3] Laboratoire Reproduction et Développement des Plantes, Univ Lyon, ENS de Lyon, UCB Lyon 1, CNRS, INRA, Inria, F-69342, Lyon, France

[*]chie.kodera@ens-lyon.fr, isabelle.fobis-loisy@ens-lyon.fr

[+]present address: Centre for Plant Sciences, Faculty of Biological Sciences, University of Leeds, Leeds, UK

Abstract:

Fertilization in flowering plants depends on the early contact and recognition of pollen grains by the receptive papilla cells of the stigma. To identify the associated molecular pathways, we developed a transcriptomic analysis based on single nucleotide polymorphisms (SNPs) present in two *Arabidopsis thaliana* accessions, one used as female and the other as male. We succeeded in distinguishing 80 % of transcripts according to their parental origins and drew up a catalog of genes whose expression is modified after pollen-stigma interaction. Global analysis of our data reveals that pattern-triggered immunity (PTI)-associated transcripts are upregulated after compatible pollination. From our analysis, we predicted the activation of the Mitogen-activated Protein Kinase 3 on the female side after compatible pollination, which we confirmed through expression and mutant analysis. Our work defines the molecular signatures of compatible and incompatible pollination, highlights the active status of incompatible stigmas, and unravels a new MPK3-dependent cell wall feature associated with stigma-pollen interaction.

29

Introduction:

31 In flowering plants, the early interaction between the tip of the female organ (stigma) and the

32 male gametophyte (pollen grain) act as a checkpoint for fertilization. This first step of the female-

33 male interaction includes recognition by the female tissues of the male partner. In the

34 Brassicaceae, sophisticated mechanisms have evolved that allow the papilla cells of the stigma to

35 reject self pollen while accepting non-self pollen. These self/non-self recognition mechanisms are

36 underlie self-incompatibility and promote genetic variability within species. Following

37 compatible pollination, the dry pollen grain starts to hydrate on the stigma papilla and ultimately

38 germinates, producing a tube that penetrates the wall of stigmatic cells and grows down to

39 convey the male gamete towards the ovules for fertilization[1,2]. By contrast, when a pollen grain is

40 recognized as incompatible, it fails to hydrate properly and shows defective germination. This

41 rejection mechanism is initiated by a ligand-receptor interaction and is genetically controlled by a

42 single polymorphic locus called the S-locus[3]. The S-locus Cysteine Rich protein (SCR)/ S-locus

43 protein 11 (SP11) located on the pollen surface interacts with its cognate S-locus Receptor

44 Kinase (SRK) localized to the plasma membrane of the papilla cells[4,5]. This interaction leads to

45 the phosphorylation of SRK that triggers the downstream cascade leading to pollen rejection[1,5,6].

46 Cellular events triggered in the stigma papillae by these two pathways, compatible and

47 incompatible, have started to be more clearly defined. Compatible pollination induces actin

48 network orientation, calcium export and polarized secretion towards the pollen grain[7–11].

49 Incompatible pollen leads to inhibition of actin polymerization and vesicular trafficking

50 accompanied by a strong calcium influx within the stigmatic cell[7,12,13]. Stigmatic calcium fluxes

51 were reported to involve the autoinhibited Ca^{2+}-ATPase13 (ACA13) for pollen acceptance[8] and a

52 glutamate receptor-like channel (GLR) for pollen rejection[12]. In addition, the stigmatic EXO70A1

53 protein was identified as a factor required for polarized secretion during compatible pollination,

54 which is negatively regulated in incompatible reaction[13,14].

55 Whereas these results help us understand specific downstream pathways, they are dependent on

56 strong *a priori*. To obtain a global picture of the early fertilization events with no *a priori*,

57 transcriptome approaches were also conducted. The main goal was to draw up catalogues of

58 genes modulated during pollination so as to unravel the stigmatic response to compatible or

2

59 incompatible pollen[8,15–18]. However, the main drawback of these approaches was the difficulty in

60 accurately distinguishing between pollen and stigma derived transcripts. To address that issue,

61 translatome analysis[19] has recently been applied to identify sex-specific genes expressed during

62 pollination, but this strategy needs great amounts of tissues from the specific transgenic line and

63 fine techniques of biochemistry.

64 Here, inspired by previous RNA-seq analysis[20], we developed a new experimental procedure

65 coupled with a bioinformatic analysis of sequencing data to comprehensively unravel the

66 dynamic events that occur both in the stigma and pollen grain following compatible and

67 incompatible pollinations. We took advantage of the SNPs existing between two distinct

68 *Arabidopsis thaliana* accessions, one used as female (Col-0) and the other as male (C24), to

69 differentiate male and female transcripts based on a new statistical methodology, ASE-TIGAR[21]

70 which can take all sequenced reads in account even those without SNPs while previous study

71 used only reads with SNPs[20]. Our analysis allowed the identification of 80 % of mRNAs

72 according to their parental origin and revealed transcriptional changes occurring specifically in

73 either the stigma or pollen grain/tube. Gene Ontology and signaling pathway prediction of up-

74 regulated genes showed that pattern-triggered immunity (PTI) pathways, including induction of

75 the Mitogen-activated Protein Kinase 3 (MPK3), were activated on the female side after

76 compatible pollination. Mutant analysis then confirmed that MPK3 is implicated in the growth of

77 pollen tubes in papilla cells.

78

Results:

Experimental setup to isolate transcripts from compatible and incompatible pollination in *A. thaliana*

82 To compare self-compatible and self-incompatible pollination, we needed to have the same

83 genetic background, albeit with different stigmatic responses to pollen. *Arabidopsis thaliana* has

84 a high level of self-fertilization due to mutations that disrupt the self-incompatibility system

85 present in its outbreeding ancestor[22]. To obtain a self-incompatible *Arabidopsis thaliana*

86 background, we transformed *A. thaliana* with a functional *SRK-SCR* gene pair isolated from its

87 close self-incompatible relative *A. lyrata*[23,24]. To analyze both compatible and incompatible

88 reactions and take advantage of nucleotide polymorphisms between *A. thaliana* accessions, we

89 generated two transgenic lines that restored the incompatible response: one in the Col-0

90 background expressing the *SRK* gene from the *A. lyrata* S14 haplotype (Col-0/*SRK14*) and the

91 other in C24 background expressing the *SCR* gene from the same *S*-haplotype (C24/*SCR14*) (Fig.

92 1a, Supplementary Fig. 1a). To express the SRK protein in stigmatic cells, we used the *SLR1*

93 promoter that displays a strong stigma-specific activity in *Brassicaceae*[25,26]. Expression of the

94 *SCR* gene was controlled by its own promoter. We selected one transgenic line for Col-0/*SRK14*

95 and one for C24/*SCR14*. Both lines were self-fertile.

96 Next, we tested the fertilization response in crosses between these lines. As expected, stigmas of

97 Col-0/*SRK14* pollinated with wild-type C24 pollen showed a clear compatible reaction with

98 hydration of pollen grains and more than 55 pollen tubes elongation on papilla cells (Fig. 1a

99 upper part, Supplementary Fig. 1bd). By contrast, when Col-0/*SRK14* stigmas were pollinated

100 with C24/*SCR14* pollen, a strong incompatible reaction was observed as deduced from poor

101 pollen hydration and the absence of pollen tube germination (Fig. 1a lower part, Supplementary

102 Fig. 1cd).

103 Building on these experimental validations, we performed a time-course experiment focusing on

104 two time-points of the interaction to identify genes whose expression is modified following

105 pollen-stigma interaction. We selected an early stage (10 minutes after pollen deposition), which

106 corresponds to the start of pollen grain hydration, and a later stage (one hour after pollination)

107 when pollen tubes reach the base of the stigma. We sequenced mRNAs extracted from pollinated

108 stigmas at 10, and 60 min after compatible (Col-0/*SRK14* x C24) pollination (C10, C60,

109 respectively) and for incompatible (Col-0/*SRK14* x C24/*SCR14*) pollination (I10, I60,

110 respectively) (Fig. 1a). We also extracted mRNA right after pollination, 0 min (Col-0/*SRK14* x

111 C24), as a control for both compatible and incompatible pollination (C0).

112

SNP-based transcriptome analysis using variants between Col-0 and C24

113

114

115 To distinguish the parental origin of the transcripts, we developed a method based on the

116 detection of small genomic variations, including SNPs and small insertions and deletions (indels)

117 between Col-0 and C24 accessions. The pipeline includes three main steps (Fig. 1b,

118 Supplementary Fig. 2). In the first step, variations between Col-0/*SRK14* and C24 genomes were

119 identified by whole-genome sequencing of the two strains with the read depth of 9.3 X for Col-

120 0/*SRK14* and 14.2 X for C24 (Supplementary Table 1). After aligning clean reads against the

121 reference genome (TAIR10, accession Col-0), SNPs and short indels between the mapped reads

122 and the reference genome sequence were identified. Reads from Col0/*SRK14* and C24 covered

123 95.8% and 90.6% of TAIR10 genome sequence, respectively. When compared to the reference,

124 the line Col-0/*SRK1*4 had 2,032 variants, while C24/*SCR14* had 732,767 variants, respectively. In

125 a second step, we introduced previously identified variants in the sequence of the TAIR10

126 template to produce two new reference genome sequences, one for Col-0/*SRK14* and one for C24

127 (Fig. 1b, Supplementary Fig.2). At the end of this process, between the new genomes of Col-

128 0/*SRK14* and C24, we identified 616,781 SNPs and 446,999 indels (Supplementary Table 2).

129 24 % and 31 % of genomic polymorphism were found in UTRs and CDSs for Col-0/*SRK14* and

130 C24, respectively, and led to sequence variations in predicted mRNAs (Supplementary Table 2).

131 We then annotated these two new genome sequences by projecting gene models from TAIR10.

132 We predicted 39,205 gene models in Col-0/*SRK14* and 39,206 in C24. We then extracted

133 predicted mRNA sequences for each gene model from these annotated Col-0/*SRK14* and C24

134 genome sequences to produce maternal and paternal reference transcripts. We obtained a list of

135 39,204 predicted gene models that were shared between maternal and paternal reference. The

136 number of predicted mRNAs with at least one SNP between Col-0/*SRK14* and C24 was 31,271

137 among the total common predicted mRNAs (39,204) (Fig. 1c). This result allowed us to

138 distinguish the origin of about 80 % (31,271/39,204 = 79.8%) of mRNAs with SNP-based

139 analysis. The last step included RNA read mapping and the estimation of sex-specific isoform

140 abundances using ASE-TIGAR. The total length of raw reads from each condition was more than

141 6,400 Mb (Supplementary Table 3). ASE-TIGAR uses a Bayesian approach to estimate allele-

142 specific expression[21]. This approach allowed us to use all sequenced reads even those without

143 SNPs. After obtaining the estimated read counts from ASE-TIGAR, we used DESeq2[27] to

144 normalize counts, for female and male transcripts, respectively (Fig. 1b, Supplementary Fig. 2

145 Supplementary Table. 4).

146   From this large dataset, we first determined the contribution of each tissue (stigma vs pollen) in

147   mixed samples harvested immediately after compatible pollination (C0). We found that among

148   the 47.0 million RNA reads, 69 % were estimated as derived from Col-0/*SRK14* (stigma), and

149   31 % were from C24 (pollen) (Fig. 1d) although 15 % of reads were assigned to the genes

150   without using SNPs. This proportion is stable over time (0, 10 min, 60 min) and independent of

151   the pollination type (compatible, incompatible), thus suggesting that these proportions are

152   reflecting the relative abundance of stigmatic cells compared with pollen grains collected by our

153   manipulation.

154   Then, we analyzed the relative abundance of each transcript between stigma and pollen. To do so,

155   transcript abundance was computed by ASE-TIGAR and was expressed as Fragments Per Kilo

156   base of exon per Million reads mapped (FPKM), which accounts for sequencing depth and gene

157   length. We then normalized FPKM (nFPKM) by dividing the FPKM of each transcript by the

158   ratio of the transcript counts from stigma [nFPKM(stigma)] or pollen [nFPKM(pollen)] at C0

159   (Fig. 1d, Supplementary Table 4). Values of nFPKM were displayed as a hexbin[28] plot to

160   visualize the distribution of gene expression levels. Genes without SNPs did not show any

161   particular pattern (Fig. 1e, bottom line). Gene expression levels were widely distributed and

162   genes highly expressed in female or in male were clearly separated, suggesting the existence of

163   distinct transcript signatures between stigma and pollen (Fig. 1e).

164

Post-validation of the SNP-based analysis

166   To have a global view of expressed genes in stigma and pollen, we constructed three classes of

167   genes from calculated nFPKM: expressed genes, sex-preferentially and sex-specifically

168   expressed genes (see methods for precise criteria of gene selection) (Supplementary Table 5).

169   Briefly, we defined genes that showed nFPKM >1 as expressed genes, those that were expressed

170   at least a ten-fold higher in stigma than in pollen as stigma-preferentially expressed genes, and

171   those that were at least one hundred-fold higher expressed in stigma than in pollen as stigma-

172   specific expressed genes (and vice versa for pollen preferentially and specifically expressed

173   genes) (Fig. 2a).

174   To evaluate the accuracy of our SNP-based analysis, we first focused on sex-specific genes and

175   analysed the top 20 highly expressed genes (Supplementary Table 5) using the ThaleMine

176   database (https://apps.araport.org/thalemine/begin.do). Heat maps of gene expression levels

177   based on Cheng et al., 2016 were generated (Supplementary Fig. 3). Interestingly, stigma specific

178   and highly expressed genes were clearly excluded from pollen even though many of them were

179   also expressed in various tissues. By contrast, most pollen specific and highly expressed genes

180   showed expression restricted to pollen and stage 12-inflorescences, which contain mature pollens

181   (Supplementary Fig.3) Moreover, within the list of stigma-specific genes, we found *AtS1*

182   (*AT3G12000.1*), which has been described as specifically expressed in *Arabidopsis* stigmas[29,30],

183   and in the list of pollen-specific genes, we found *CPK34* (*AT5G19360.*1), the protein product of

184   which is involved in pollen tube regulation[31]. Finally, to confirm the specific expression of these

185   genes in stigma or pollen, we carried out RT-PCR and sequence the cDNAs of SNP-containing

186   regions using C0 sample as template. From the top 20 highly expressed genes, we selected genes

187   whose location of SNPs permitted designing of primers. We found that, as expected, mRNAs of

188   genes in the stigma-specific genes had SNPs only from Col-0/*SRK14* (stigma), whereas mRNAs

189   of genes in the pollen-specific genes had SNPs only from C24 (pollen) SNPs (Fig. 2b).

190   To assess the global consistency of our data sets with already published studies, we further

191   analyzed our SNP-based data by correlating them tissue-specific transcripts reported from

192   microarray experiments[32–34]. Stigma associated transcripts from our analysis showed poor

193   correlation with male transcriptomes from mature pollen or growing pollen tube, whereas the

194   highest correlation was observed with transcriptome from unpollinated stigmas. Conversely, our

195   pollen associated transcriptome showed a high correlation with male transcriptomes and only

196   poorly correlated with female transcriptomes or transcriptomes from vegetative tissues (Fig. 2c).

197   Correlations between another recent SNP-based analysis, which identified pistil- and pollen tube-

198   specific transcripts 8 hour after pollination[20] and the tissue/organ-specific transcripts showed

199   similar trends to our stigma- and pollen-transcripts (Fig. 2c).

200   To further characterize the pollen vs. stigma associated transcripts, we looked for Gene Ontology

201   (GO) term enrichment at C0 within the list of sex-preferentially expressed genes (FDR < 0.05).

202   Although GO terms may be somewhat subjective or not fully consolidated by functional tests,

203   with the current annotation, we observed a clear difference between the two sets of transcripts

204   (Fig. 2d). From GO term enrichment of the top 1000 highly expressed genes among stigma or

205   pollen -preferentially expressed genes (Supplementary Table 5, Supplementary Table 6), our

206   analysis revealed high enrichment of several GO terms associated with metabolism in stigmas

207   (such as "photosynthesis", "mitochondrial-", and "-metabolic process") suggesting an active

208   metabolic state of stigmatic cells (Fig. 2d left). Conversely, GO terms on the pollen side were

209   specific to pollen functions such as "pollen tube growth", "pollen sperm cell differentiation" and

210   "cell tip growth" (Fig. 2d right).

211   Osaka et al.[35] previously reported the transcriptome of unpollinated stigmas using laser

212   microdissection of *Arabidopsis* stigmatic cells. Among the top 100 expressed genes in this latter

213   analysis, 44 were common with the top 100 expressed genes in stigma of our analysis at C0[35].

214   Altogether, these results validate our SNP-based workflow, which allows identification of

215   female- and male- derived transcripts from a combination of tissues following pollination.

216

Gene expression dynamics triggered after pollination

218   To examine the transcriptomic response of pollen and stigma following compatible or

219   incompatible pollination, we first performed a principal component analysis (PCA) [36] using the

220   gene expression levels of each biological replicate in all conditions (Fig. 3a). Data from stigma-

221   and pollen-transcripts were treated separately (Fig. 3a left and right, respectively). The total

222   explained variance of the first two principal components (PC1 and PC2) is around 39% (28 +11)

223   for stigma and 35% (24 + 11) for pollen. These relatively low percentages are explained by the

224   fact we took all genes and not only those that are specific for compatible or incompatible

225   reaction. It also explain the fact that the different conditions (C0, C10, C60, I10 & I60) were not

226   always well separated along those axis.

227   Nevertheless, comparing the PCA of stigma and of pollen transcripts suggested different

228   dynamics in each tissue. On the stigma side, the PCA showed that both compatible and

229   incompatible pollinations triggered a transcriptional response. Along the PC1 axis, capturing

230   almost 30% of the explained variance, samples are temporally sorted from 0 min to 60 minutes,

231   thus suggesting that PC1 can be interpreted as a time-axis. For the second axis, explaining 14%

232   of the observed variability, compatible samples are located in the lower part when incompatible

233   samples are located in the upper part, close to those of the starting point (C0). This seems to

234   indicate that this axis is oriented by the compatible/incompatible effect. Meanwhile, on the

235   pollen side, all the conditions except C60 were clustered together. Again PC1 captures the

236   temporality of the compatible response, however we cannot conclude that PC2 is related to the

237   compatible response effect since early compatible and incompatible clusters overlap.

238   The clear response pattern of pollen at 1 hour is coherent with the massive changes displayed by

239   compatible pollen, which hydrated and germinated a pollen tube growing in the stigmatic tissue

240   (Fig. 3a).

241   After performing differentially expressed gene (DEG) analysis, we found more up regulated

242   genes than down regulated genes, and more DEGs in stigma than in pollen (1841 up in stigma vs.

243   595 in pollen, 513 down in stigma vs. 113 down in pollen) (Supplementary Table 7). To get a

244   clearer picture on the number of genes whose expressions were modified during the course of

245   pollination, we then used a Venn diagram representation (Fig. 3b) only with up regulated genes

246   (padj < 0.1, FC > 2) to study. The Venn diagram of up-regulated genes in stigma (Fig. 3b left)

247   showed similar dynamics to those observed in PCA, with a moderate alteration of gene

248   expression in incompatible reactions, with only 45 genes at I10 and 344 genes at I60. By contrast,

249   following compatible pollination, a massive and progressive change of gene expression was

250   detected with 414 up-regulated genes at C10 and 1038 at C60 (Fig. 3b left). On the pollen side

251   (Fig. 3b right), very few genes showed altered expression, except in condition C60, where 551

252   genes were up-regulated (6 common in C10 and C60, 533 exclusively in C60) (Supplementary

253   Table 8). Again this correlates perfectly with the PCA. Although the pollen is completely

254   changing its physiology during compatible pollination, the stigma does not remain passive and

255   undergoes a massive molecular reprogramming.

PTI pathways induced after compatible pollination in stigma

257   The rapid and global transcriptomic changes in stigma after compatible pollination motivated us

258   to investigate the molecular events occurring at this stage. The 944 genes (158 + 163 + 623)

259   induced only after compatible reaction (Fig. 3b left) showed dramatically different GO terms and

260   enrichment from those preferentially expressed at C0 in the stigma (Fig. 2d left, Fig. 3c). There

261   were 126 terms with high confidence (FDR < 0.05) and 85 terms with FDR < 0.005

262 (Supplementary Table 9). In particular, we found many GO terms including "response" and

263 "signalling", thus suggesting the prompt activation of signalling pathways in response to the

264 pollination event. We also applied the enrichment analysis for 108 genes (104 + 4) that were

265 induced only after incompatible pollination in stigma. But this was not informative when

266 compared with compatible reaction as only 9 terms showed a FDR < 0.05 with the minimum

267 FDR = 0.006.

268 To predict induced pathways after pollination, we then mapped the 944 up-regulated genes after

269 compatible pollination to KEGG pathways[37]. We found many metabolism related pathways,

270 signaling pathways including hormone-signaling (with 20 genes), plant-pathogen interaction

271 (with 22 genes) and MAPK pathways (with 11 genes). Interestingly, two plant-pathogen

272 interaction pathways known as pattern-triggered immunity (PTI) induced by bacterial flg22 and

273 EF-Tu[38] were clearly distinguishable with 5 up-regulated genes in compatible situation (Fig. 4,

274 green). On the other hand, among the 108 (4+104) exclusively up-regulated genes after

275 incompatible pollination, we could not distinguish clear induction of PTI pathways as only one

276 gene, *EFR*, was up-regulated (Fig. 4, gray).

277 In the compatible pollination, *SERK4*, *BAK1*, *EFR* and *FLS2* - all genes known to encode

278 receptors of bacterial components - were expressed in stigma at C0 and *SERK4* was up regulated

279 at C60 (FC = 2.3). Although *MKK6* and the transcription factor-encoding genes *WRKY22* and

280 *WRKY25* were not expressed at C0, the first two were already induced at C10 and induction was

281 maintained at C60, while *WRKY25* was induced only at C60 (all FCs were between 2 and 2.8).

282 *MPK4* and *MPK6* were highly expressed from C0 to C60 compared with other components of the

283 pathway but did not exhibit significant expression change. Interestingly, even though *MPK3*,

284 *WRKY33* and *WRKY53* did not have SNPs, their high induction following compatible (FC = 6.3,

285 10.0, 11.0 respectively) compared with incompatible (FC = 1.5, 2.8, 5.2) reaction suggests that

286 this PTI pathway is a hallmark of compatible pollination (Fig. 5, Supplementary Table. 10).

287 Altogether, these analyses indicate that the PTI pathway is rapidly induced in stigma only after

288 compatible pollination.

289

Stigma-pollen interaction activates and requires MPK3

291   The predicted mRNA of *MPK3* did not have SNPs between Col-0/*SRK14* and C24, preventing

292   the accurate assignment of the increased expression to stigma tissues. To check whether

293   activation of MPK3-associated pathways occurs in stigma, as predicted from our analysis, we

294   derived the list of genes known to be co-expressed with MPK3 from ATTED-II

295   (http://atted.jp/)[39]. Genes in the list were ordered based on Pearson's correlation coefficient with

296   MPK3 expression (from high to low) (Supplementary Table 11). After removing the genes

297   without SNPs, we checked the expression of the top 50 genes using our SNP-based analysis in

298   stigma (Supplementary Fig. 4, upper plot) and pollen (Supplementary Fig. 4, lower plot). At C0,

299   most of the genes were moderately expressed in stigma but not in pollen. After compatible

300   pollination, they were induced only in stigma, supporting our hypothesis of a stigma-specific

301   MPK3 pathway induction. Subsequently, we took advantage of the MPK3-knockout line *mpk3-*

302   *DG*[40–42] to monitor the expression and activation of MPK3 protein *in vivo*.

303   Immunoblotting was performed on protein extracts of pollinated stigmas from the following

304   combinations of crosses: Col-0 x *mpk3* (i.e., MPK3 protein only present in stigma), *mpk3* x Col-0

305   (i.e., MPK3 only in pollen), Col-0 x Col-0 (MPK3 in both), and *mpk3* x *mpk3* as a negative

306   control. Pollinated stigmas were harvested immediately or 60 min after pollination,

307   corresponding to C0 and C60, respectively. The absence of a specific band for MPK3 from the

308   *mpk3* x *mpk3* sample confirmed the complete knockout of the mutant (Fig. 6a). MPK3 protein

309   was detected in both stigma (Col-0 x *mpk3*) and pollen (*mpk3* x Col-0) but with a higher

310   abundance in the stigma (Fig. 6ab). MPK3 was slightly accumulated 60 min after pollination in

311   stigma and in pollen (FC = 1.6 and 2.4, respectively). Subsequently, we checked whether MPK3

312   was activated through phosphorylation using an anti-Phospho MPK antibody. At C0, the band

313   corresponding to phosphorylated MPK3 was very weak, but its intensity clearly increased after

314   compatible pollination in stigma but not in pollen (FC = 5.2 and 0.9 respectively) (Fig. 6cd).

315   Altogether these results demonstrate that MPK3 is both transcriptionally and post-translationally

316   activated in the stigma during compatible pollination.

317   To elucidate whether the loss of MPK3 function might have any effect on pollen-stigma

318   interaction, we pollinated *mpk3* stigmas with Col-0 pollen and observed the pollinated stigmas 60

319   min after pollination by scanning electron microscopy. Col-0 x Col-0 pollination was used as a

320   control. Before pollination, there were no apparent differences between stigmas of *mpk3* and Col-

321   0 (Supplementary Fig. 5). Hydration of pollen grains and elongation of pollen tubes occurred

322   normally on *mpk3* stigmas compared to the control. However, when we measured the width of

323   the contact sites between the pollen tube and stigma (white arrows on Fig. 7a), even if the

324   distributions of the values were partly overlapping we found that contact sites were significantly

325   wider on *mpk3* stigmas compared with Col-0 (Fig. 7b). This demonstrates that MPK3 contributes

326   to the stigma-pollen interaction and structure.

327

Discussion:

329   To decipher the mechanisms that control reproduction in flowering plants, we extracted the

330   global transcriptomic signatures associated with both pollen and stigmatic cells following their

331   interaction during compatible or incompatible pollination. Although transcriptomes of pollinated

332   stigmas have been recently published[17,18], these analyses did not try to distinguish between pollen

333   and stigma transcripts. In the present work, we provide a comprehensive transcriptomic dataset

334   for stigma-pollen interactions using a novel SNP-based analysis. We took advantage of a recently

335   developed statistical tool called ASE-TIGAR, which is based on a Bayesian approach to estimate

336   allele-specific expression in diploid cells[21]. Nariai et al. showed an accurate estimation of gene

337   expression from RNA-seq with ASE-TIGAR and identified some autosomal genes as allele-

338   specific genes in a human reference lymphoblastoid cell line. We applied this new tool to

339   discriminate transcripts from female-male mixed tissues during the first steps of the fertilization

340   process. Our experimental design and bioinformatic pipeline allowed us to unveil the

341   transcriptomic response of the pollen/pollen tube and that of the stigma following compatible or

342   incompatible pollination at two early (10 min and 60 min) time points of the male-female

343   interaction (Fig. 1). It is worth noting that another SNP-based pipeline has recently been

344   published[20], identifying transcripts derived from the pistil and pollen tubes collected 8h after

345   compatible pollination. Although we cannot compare the two analyses directly, as pollination

346   time points were different and only compatibility was studied by Leydon et al., both analyses

347   succeeded in distinguishing male and female transcripts as presented in Fig. 2c. However, while

348   Leydon et al., 2017 used 12 % of reads that had SNPs among the total sequenced reads, in our

349   analysis we took all the RNA-seq reads into account, including those without SNPs[20,21]. This

350   difference in the approaches has likely contributed to making our analysis more exhaustive, as

351 exemplified by the remarkable segregation we found between male transcripts and those derived

352 from female and vegetative tissues (Fig.2 c). The sex preferentially- or specific-expressed gene

353 lists we drew up contain many of the already identified female or male specific genes and

354 reported GO term enrichment[8,13,14] (Fig.2). Our analysis also clarified the expression of genes that

355 have been reported to have function during pollination. The exocyst complex, including the

356 EXO70A1 protein, has been shown to play a role in pollen acceptance, probably through its

357 function in the secretion of factors required for pollen hydration and pollen tube growth[13,14]. We

358 found *EXO70A1* to be stably expressed in stigmas over time (nFPKM(stigma) = 27.1 at C0, with

359 no expression change following pollination). *ACA13* which was shown to be involved in calcium

360 fluxes was up-regulated after both compatible (FC=3.2 at C60) and incompatible (FC=2.4 at I60)

361 pollinations; similar up-regulation after compatible pollination was also reported by Iwano et al.,

362 2014.

363 Together with the correlation analysis (Fig. 2c) and experimental evaluations (Fig. 2b) we can

364 conclude that our female- / male-transcripts globally represent stigma-/pollen-transcripts.

365 Transcriptomic dynamics shown by PCA and Venn diagrams were not substantial in terms of

366 variance and number of DEGs (Fig. 3ab). These results are in line with those of Matsuda et al.[17]

367 who reported only a few percent of difference between transcripts before and 60 min after

368 pollination for both compatible and incompatible interactions.

369 While our data are rather consistent with other transcriptomic analyses of pollinated stigmas[8,17,35]

370 (Fig. 2, 3), the clear distinction we made between male and female transcripts also reveals

371 surprises. The Venn diagram suggested a rapid transcriptomic response in the stigma for

372 compatible (414 up-regulated genes at C10) but not for incompatible pollination (45 up-regulated

373 genes at I10) (Fig. 3b left). Since almost no specific transcriptional induction was detected at I10

374 (only 4 up-regulated genes), this suggests that key molecules required for the incompatibility

375 reaction are already present in the stigma (Fig.3b left, I10up). This may be consistent with the

376 observation that the pollen rejection response in *A. thaliana* lines exhibiting a restored

377 incompatibility system is extremely rapid and occurs within minutes[12]. Astonishingly, while no

378 cellular changes were detectable by SEM on stigmas one hour after incompatible pollination (Fig.

379 1a), we identified more than one hundred up-regulated genes in stigmas and only 6 in pollen at

380 I60 (Fig. 3b). This demonstrates that the stigma undergoes major molecular changes following

381 incompatible pollination, i.e. that incompatibility is actively maintained through a global

382 physiological modification of the stigmatic cells. The stigma up-regulated genes can be

383 assimilated to the stigmatic response to self-incompatible pollen. As the incompatibility reaction

384 is maintained for several days, at least as long as SRK is properly expressed in the stigma, we

385 may propose that among the stigma up-regulated genes there are key factors required for the

386 maintenance of SI. Since components of the signaling pathway downstream of the SRK-

387 SP11/SCR receptor-ligand complex are still not fully unveiled, our data provide a key resource to

388 identify new genes involved in the incompatibility response and its maintenance over time.

389 Our results revealed a molecular signature of compatible pollination in stigma involving the

390 activation of stress response genes and PTI pathways (Figs. 3, 4, 5). The similarity between the

391 stigma-pollen interaction and plant-pathogen interaction has been discussed and has drawn

392 researchers' attention for a long time[10,43–45]. Several transcriptomic analyses of pollinated

393 stigmas/pistils reported enrichment in transcripts linked to stress or defense response in female

394 tissues[18,20,34,45,46]. Tung et al. and Leydon et al. suggested that such defense-related genes could

395 have functions in pollination. Moreover, although incompatible response has been considered to

396 share common mechanism with plant-pathogen interaction as it is a response to block the

397 invader[18,45], in our analysis, GO terms associated with defense responses did not clearly appear

398 after incompatible pollination but rather were mainly associated with the compatible response

399 (Fig. 3c).

400 Recently, Zhang et al.[18] performed a time course transcriptome analysis of compatible and

401 incompatible reaction in *Brassica napus*. They speculated that compatible responses had close

402 parallels with plant-pathogen interactions, mainly with effector-triggered susceptibility, while

403 incompatible response rather resembled effector-triggered immunity, and that PTI could be

404 common to both compatible and incompatible responses. Although we found up-regulated

405 defense related genes in the incompatible reaction, no clear defense pathways were identified by

406 KEGG analysis. By contrast, our study clearly indicates that two PTI pathways were induced

407 during compatible response (Fig.4). Indeed, the SNP-based analysis demonstrated the stigma

408 specific expression and induction of genes involved in these pathways (Fig. 5). This result was

409 not completely unexpected since pollen tube growth resembles pathogen attack from several

410 angles, for example invasive growth recognition of an external invader, cell wall digestion, and

411   calcium burst[8,47,48]. We suggest that plant responses to pollen and pathogens share conserved

412   molecular mechanisms at early stages of the interactions but that later downstream deviations

413   could lead to different reactions, one inhibiting pathogen invasion, while the other promotes

414   pollen tube growth in the pistil. Because links between symbiotic and pathogen interactions have

415   been already been uncovered[49,50], we can also speculate that the response of plant cells to

416   symbiotic organisms could share common mechanisms with the response of the stigma to pollen.

417   How these shared modules evolved together whilst maintaining highly specific responses (i.e.

418   pollination, PTI, symbiosis) is an intriguing question for future studies.

419   MPK3 is one of the key components of PTI signaling pathways[38], and we confirmed both the

420   induction of genes associated with MPK3 expression, and MPK3 activation itself, in compatible

421   pollinated stigmas (Supplementary Fig. 4, and Fig. 6). The increased pollen-stigma contact sites

422   we observed in *mpk3* mutant suggest that the structural properties of the cell wall in the mutant

423   could somehow be impaired (Fig. 7). Although the role of mechanical signals and cell wall

424   reorganization has been studied in growing pollen tubes *in vitro*[51–53], very little is known about

425   components involved in pollen tube penetration and elongation within the stigma. It seems likely

426   that major cell wall modifications are necessary to allow pollen tube growth through softening

427   and loosening of the cell matrix[48]. How the pollen tube and stigma papilla contribute to these

428   changes is still unknown even though both male and female partners are likely to contribute. The

429   identification of a MPK3-dependent stigma-pollen interaction structure provides an interesting

430   phenotypic indicator for such future studies.

431   MPK3 is involved in sensing cell wall modifications and reorganization during development as

432   well as following the perception of external signals like pathogen attacks and wounding by

433   receptor-like Wall-Associated Kinases (WAKs)[54,55]. WAKs bind pectin fragments and

434   oligogalacturonic acids that are generated by pathogen attacks and wounding. In stigmas, two of

435   the *WAK* family members (*AT2G23450* and *AT1G79670*) were stably expressed (nFPKM(stigma)

436   = 11.7 and 12.2, respectively at C0 with no expression change following pollination), and another

437   member, *AT1G21210*, was up-regulated after compatible pollination (FC = 2.3 at C60).

438   Interestingly, Glycine-Rich Protein3 (GRP3), a possible ligand for WAKs that is known to bind

439   to WAK1[56] was highly expressed (nFPKM(stigma) = 303.0 at C0 and no expression change

440   following pollination) in stigmas. In addition, we found that several pectin related enzymes were

15

441   up-regulated in stigmas after compatible pollination. Taken together, we propose that cell wall

442   reorganization that allows pollen tube growth in the stigma could be dependent on MPK3-based

443   pathways (Fig. 8).

444   Our study elucidates the molecular signatures of pollen and stigma responses following pollen-

445   stigma interaction in compatible and incompatible situations. Most remarkably, we reveal that the

446   acceptance of pollen grains involves the activation of PTI pathways and we confirm the long-

447   suspected idea that fertilization and plant pathogen responses share common molecular signaling

448   components.

449

Materials and Methods:

451   *A. lyrata SCR14* and *SRK14* gene cloning and plasmid construction

452   We used Gateway® vectors[57] (Life Technologies, USA) for expression of transgenes in

453   *Arabidopsis thaliana*. The *AlSRK14* genomic sequence spanning the coding region from the start

454   to the stop codons (3,620 kb) was amplified from genomic DNA of an *Arabidopsis lyrata*

455   individual containing the *S14*-locus with specific AttB-containing primers

456   (5'GGGGACAAGTTTGTACAAAAAAGCAGGCTACCATGAGAGGTGTAATACCAAAGT

457   ACC3' and

458   5'GGGGACCACTTTGTACAAGAAAGCTGGGTTTACCGAGGTTCCACTTCCGTGGTGG3'

459   ) and subsequently inserted by BP recombination into a pDon207 plasmid. A fragment of 4,081

460   kb containing the *AlSCR14* gene, 1,844 kb of the 5' upstream region and 817 bp of the 3'

461   downstream region were amplified from genomic DNA of *Arabidopsis lyrata* individual

462   containing the *S14*-locus using the AttB-containing primer

463   (5'GGGGACAAGTTTGTACAAAAAAGCAGGCTCGGGTAGCTCAACCTAGCTAAG3' and

464   5' ACCACTTTGTACAAGAAAGCTGGGT CATGATCACCAAAGACAAGATCC3'). This

465   fragment was subsequently inserted by BP recombination into a pDONR-Zeo plasmid. The DNA

466   fragment containing the *Brassica oleracea SLR1* promoter (1.5 kb upstream of the *SLR1* start

467   codon[25,26]) was inserted into a the pDONR P4-P1R plasmid[58]. The *SLR1* promoter, the genomic

468   sequence *AlSRK14* and a 3'mock sequence were inserted in the pK7m34GW destination vectors

469   by three fragment LR recombination. The genomic sequence *AlSCR14*, a 5'mock sequence and a

16

470   3'mock sequence were inserted in the pB7m34G. GenBank accession numbers for pg*AlSCR14*

471   (promoter and gene of *AlSCR14*) and p*SLR1*-g*AlSRK14* (*SLR1* promoter and *AlSRK14* gene) are

472   MH680584 and MH680585, respectively.

Plant material and growth condition

474   *Arabidopsis thaliana* C24 and Col-0 transgenic plants were generated using *Agrobacterium*

475   *tumefaciens*-mediated transformation according to Logemann et al. 2006[59]. *AlSRK14* construct

476   was introduced in Col-0 (Col-0/*SRK14*). *AlSCR14* construct was introduced in C24 (C24/*SCR14*).

477   Unique insertion lines homozygotes for the transgene were selected. mpk3-DG[40–42] was kindly

478   gifted from Marcel Wiermer and Yuelin Zhang. All plants including Col-0 and C24 were grown

479   in growth chambers under long-day cycles (16h light/8h dark at 21°C/19°C).

Aniline blue staining and observation

481   Buds at the end of stage 12[60] were emasculated and 18 hours later, stigmas which have reached

482   the stage 13 or Early 14 (14E), were pollinated with mature pollen grains. After 2 h, pollinated

483   stigmas were fixed in acetic acid 10%, ethanol 50% and stained with Aniline Blue for

484   epifluorescence microscopy observation. Germinated pollen grains with pollen tubes within the

485   stigmas were manually counted. We considered that pollination is incompatible when fewer than

486   5 pollen tubes were able to overcome the stigmatic barrier[61].

487

Genomic DNA and mRNA preparation

489   For genomic DNA extraction, about 2 mL volume young inflorescences of Col-0/SRK14 and

490   C24 were harvested, respectively. After grinding the material in liquid nitrogen, DNA was

491   extracted as described previously[62]. For RNA extraction, late stage 12[60] Col-0/SRK14 flowers

492   were emasculated and 16-20h after emasculation stigmas were pollinated with compatible (C24)

493   or incompatible pollen (C24/*SCR14*). 0, 10 or 60 minutes after compatible pollination (C0, C10

494   and C60) or incompatible pollination (I10, I60), 50 stigmas were harvested manually using fine

495   tweezers, then frozen in liquid nitrogen and stored at − 80 °C until further processing. After

496   grinding the material in liquid nitrogen, RNA was extracted and purified by using Arcturus®

497   PicoPure® RNA Isolation Kit (Applied Biosystems / Thermo Fisher Scientific) following the

498   manufacturer instruction except that we added a DNAse treatment (Qiagen, catalog#79254). Five

17

499 biological replicates of RNA at each point were prepared then four replicates were selected for

500 sequencing based on their quality and quantity.

Whole genome sequencing and variant calling

502   Library preparation and whole genome sequencing of Col-0/SRK14 and C24 were performed by

503 HELIXIO (Clermont-Ferrand, France; http://www.helixio.com/) with TruSeq® DNA PCR-free

504 Library Preparation kit (Illumina) and NextSeq500 platform (Illumina) applying paired-end

505 sequencing (2×150 bp) (Supplementary Table 1). We then proceeded to the analysis of the

506 sequencing data using GATK3.5 after quality check by FastQC

507 (http://www.bioinformatics.babraham.ac.uk/projects/fastqc), trimming and pairing of the

508 resulting reads using custom Perl scripts. We aligned the reads to the Col-0 reference genome

509 (TAIR10) with BWA[63], applied GATK[64] base quality score recalibration, indel realignment,

510 duplicate removal, and performed SNP and INDEL discovery across all samples according to

511 GATK Best Practices recommendations[65,66]. After checking the depth of coverage of two samples

512 by using GATK DepthOfCoverage (Supplementary Fig. 6), we performed filtering applying

513 depth 3 for Col-0/SRK14 and depth 6 for C24 and homozygous for both, then obtained the

514 complete set of variants for each genome as VCF files.

Production of new reference genomes

516 Col-0/SRK14 and C24 genome sequences were derived from TAIR10 genome, by introducing

517 the called variants in the sequence, by using GATK FastaAlternateReferenceMaker. Gene

518 annotations from TAIR10 genome were transferred onto the two new genome sequences using

519 RATT[67] in "Strain" mode and seqret from EMBOSS suite[68]. To characterize polymorphism

520 (SNPs and short indels) between obtained Col-0/SRK14 and C24 genome sequences, inside and

521 outside predicted genes, we aligned chromosome sequences using LAST (v. 938)[69], after training

522 LAST on chromosomes 1.

RNA sequencing and expression analysis

524 Library preparation and RNA sequencing were performed by HELIXIO with TruSeq® Standard

525 mRNA sample Preparation kit (Illumina) and NextSeq500 platform (Illumina) applying paired-

526 end sequencing (2x75 bp). We then proceeded to the analysis of the sequencing data using ASE-

527 TIGAR after quality check by FastQC, trimming and pairing of the resulting reads using custom

18

528 Perl scripts. First, we derived mRNA reference sequences from new reference genomes and

529 merged them in one FASTA file, then mapped the clean reads on the mRNA reference with

530 Bowtie2[70]. We then run ASE-TIGAR with SAM files produced by mapping and the mRNA

531 reference[21] (http://nagasakilab.csml.org/ase-tigar/). Raw sequencing data is available at NCBI

532 database (https://www.ncbi.nlm.nih.gov/sra/SRP154565) under SRA accession: SRP154565.

Comparison with published datasets

534 To check the consistency of our RNA-seq data with previously published microarray data[32–34],

535 for each pair of condition, we computed a Pearson correlation coefficient (r) over all genes with

536 SNPs from our variant analysis, using mean of estimated read counts from three or four

537 biological replicates for RNA-seq and mean absolute intensity for multiple microarray replicates.

538 We also computed Pearson correlation coefficients (r) between previously published RNA-seq

539 data[20] and the microarray data sets.

Differential gene expression analysis and calculation of nFPKM.

541 Differential expression analysis on the whole transcriptome was performed using DESeq2[27].

542 After performing principal component analysis (PCA) for all biological replicates at each

543 condition, we removed one replicate at I10 from female samples and one at I60 from male

544 samples, as they were isolated from their other replicates. All the analyses, including the

545 presented PCA, were performed with the sample set after the removal.

546 Normalized FPKM (nFPKM) was calculated by dividing stigma- or pollen-FPKM by female or

547 male transcript proportion at each condition (C0, C10, C60, I10, I60).

548

Criteria to select expressed genes, sex–preferentially or specifically expressed genes

550 To select expressed genes, sex-preferentially or specifically expressed genes at C0 (Fig. 2a,

551 Supplementary Table 5), we used nFPKM. We defined stigma-expressed genes consisting

552 [nFPKM(stigma) >1 $\cap$ with SNPs] and stigma-preferentially expressed genes consisting

553 [nFPKM(stigma) > 1 $\cap$ nFPKM(stigma) $\geq 10 \times$ nFPKM(pollen)]. Sex-specifically expressed

554 genes were selected among sex-preferentially expressed genes applying more stringent criteria.

555 Stigma-specifically expressed genes consist [stigma preferentially expressed genes $\cap$

556 nFPKM(pollen) $\leq 1 \cap$ nFPKM(stigma) $> 100 \cap$ nFPKM(stigma) > 100 x nFPKM(pollen)], then

557 sorted by nFPKM(stigma) from the largest to the smallest. Vice-versa for pollen (preferentially /

558 specifically) expressed genes

GO term and enrichment analysis and pathway analysis

560   GO and gene enrichment analyses were performed using Gene Ontology Consortium website

561 (http://www.geneontology.org/) and PANTHER13.1 software[71,72]. We used "GO biological

562 process complete" for the classification. GO terms with False Discovery Rate (FDR) < 0.05 were

563 considered as significantly enriched.

564   Pathway analysis was performed using and KEGG PATHWAY Database using KEGG Mapper

565 software (http://www.kegg.jp/kegg/tool/map_pathway2.html)[37].

RT-PCR and sequencing

567 For experimental evaluation of the SNP-based analysis with reverse transcription polymerase

568 chain reaction (RT-PCR) and sequencing, we selected genes among the top-20 specifically

569 expressed genes that have SNPs at suitable positions allowing discrimination of parental origin

570 (stigma vs pollen) (Fig. 2b). RNA at C0 was purified as described above. cDNA was generated

571 using SuperScript® VILO™ cDNA Synthesis Kit (Invitrogen). Primers were designed by

572 Primer3web (http://bioinfo.ut.ee/primer3/) at the flanking region of SNP including sites. PCR was

573 performed with GoTaq (Promega). PCR products were purified using PCR clean-up Gel

574 extraction kit (Macherey-Nagel) and then sequenced.

Protein extraction and western blotting

576   Proteins from around 50 pollinated stigmas at C10 and C60 were extracted in SDG buffer (Tris-

577 HCl 62.5 mM pH 6.8, Glycerol 10%, DTT 2%, SDS 2.5 %). Proteins were separated on a 10 %

578 SDS-PAGE gel and immunodetected with Anti-AtMPK3 (Sigma, M8318), anti-phospho p44/p42

579 MAPK (Cell Signaling, #9101S), or anti-alpha-Tubulin (Sigma, T5168). Band intensities were

580 normalized to tubulin signal using ImageJ software.

Environmental Scanning Electron Microscopy (SEM).

582 Late stage 12 stigmas were pollinated with mature Col-0 pollen and 60 min after pollination,

583 stigmas were observed under Hirox SEM (SH-3000 table-top) at -20 °C with an accelerating

584   voltage of 10 kV. The width of each pollen tube–stigma contact site was measured using ImageJ

585   sofware. We applied a Student test to the measurements.

586

References:

588   1. Doucet, J., Lee, H. K. & Goring, D. R. Pollen Acceptance or Rejection : A Tale of Two Pathways. *Trends*

589   *Plant Sci.* **21,** 1058–1067 (2016).

590   2. Mizuta, Y. & Higashiyama, T. Chemical signaling for pollen tube guidance at a glance. *J Cell Sci* **131,**

591   jcs208447 (2018).

592   3. Bateman, A. J. Self-incompatibility systems in angiosperms. *Heredity* **9,** 52–68 (1955).

593   4. Kachroo, a, Schopfer, C. R., Nasrallah, M. E. & Nasrallah, J. B. Allele-specific receptor-ligand

594   interactions in Brassica self-incompatibility. *Science* **293,** 1824–1826 (2001).

595   5. Takayama, S. *et al.* Direct ligand-receptor complex interaction controls Brassica self-incompatibility.

596   *Nature* **413,** 534–538 (2001).

597   6. Cabrillac, D., Cock, J. M., Dumas, C. & Gaude, T. The *S*-locus receptor kinase is inhibited by

598   thioredoxins and activated by pollen coat proteins. *Nature* **410,** 220–223 (2001).

599   7. Iwano, M. *et al.* Actin dynamics in papilla cells of Brassica rapa during self- and cross-pollination. *Plant*

600   *Physiol.* **144,** 72–81 (2007).

601   8. Iwano, M. *et al.* A pollen coat-inducible autoinhibited Ca2+-ATPase expressed in stigmatic papilla cells

602   is required for compatible pollination in the Brassicaceae. *Plant Cell* **26,** 636–49 (2014).

603   9. Elleman, C. J. & Dickinson, H. G. Pollen-stigma interactions in Brassica. IV. Structural reorganization in

604   the pollen grains during hydration. *J. Cell Sci.* **80,** 141–157 (1986).

605   10.   Elleman, C. J. & Dickinson, H. G. Identification of pollen components regulating pollination-

606   specific responses in the stigmatic papillae of Brassica oleracea. *New Phytol.* **133,** 197–205 (1996).

607   11.   Safavian, D. & Goring, D. R. Secretory Activity Is Rapidly Induced in Stigmatic Papillae by

608   Compatible Pollen, but Inhibited for Self-Incompatible Pollen in the Brassicaceae. *PLOS ONE* **8,** e84286

609   (2013).

610   12.   Iwano, M. *et al.* Calcium signalling mediates self-incompatibility response in the Brassicaceae.

611   *Nat. Plants* **1,** 1–8 (2015).

612   13.   Safavian, D. & Goring, D. R. Secretory activity is rapidly induced in stigmatic papillae by

613   compatible pollen, but inhibited for self-incompatible pollen in the brassicaceae. *PLoS ONE* **8,** (2013).

614   14.   Indriolo, E., Safavian, D. & Goring, D. R. The ARC1 E3 Ligase Promotes Two Different Self-Pollen

615   Avoidance Traits in Arabidopsis. *Plant Cell* **26,** 1525–1543 (2014).

616   15.   Swanson, R., Edlund, A. F. & Preuss, D. Species Specificity in Pollen-Pistil Interactions. *Annu. Rev.*

617   *Genet.* **38,** 793–818 (2004).

618   16.   Sankaranarayanan, S., Jamshed, M. & Samuel, M. A. Proteomics Approaches Advance Our

619   Understanding of Plant Self-Incompatibility Response. *J. Proteome Res.* **12,** 4717–4726 (2013).

620   17.   Matsuda, T. *et al.* Transcriptional Characteristics and Differences in Arabidopsis Stigmatic Papilla

621   Cells Pre- and Post-Pollination. *Plant Cell Physiol.* **56,** 663–673 (2015).

622   18.   Zhang, T. *et al.* Time-Course Transcriptome Analysis of Compatible and Incompatible Pollen-

623   Stigma Interactions in Brassica napus L. *Front. Plant Sci.* **8,** 682 (2017).

624   19.   Lin, S.-Y. *et al.* Profiling of translatomes of in vivo-grown pollen tubes reveals genes with roles in

625   micropylar guidance during pollination in Arabidopsis. *Plant Cell* **26,** 602–18 (2014).

626   20.   Leydon, A. R. *et al.* The molecular dialog between flowering plant reproductive partners defined

627   by SNP-informed RNA-Sequencing. *Plant Cell* **29,** 984–1006 (2017).

628   21.   Nariai, N., Kojima, K., Mimori, T., Kawai, Y. & Nagasaki, M. A Bayesian approach for estimating

629   allele-specific expression from RNA-Seq data with diploid genomes. *BMC Genomics* **17,** 2 (2016).

630   22.   Tsuchimatsu, T. *et al.* Evolution of self-compatibility in *Arabidopsis* by a mutation in the male

631   specificity gene. *Nature* **464,** 1342–1346 (2010).

632   23.   Kusaba, M. *et al.* Self-incompatibility in the genus Arabidopsis: characterization of the S locus in

633   the outcrossing A. lyrata and its autogamous relative A. thaliana. *Plant Cell* **13,** 627–643 (2001).

634   24.   Nasrallah, M. E., Liu, P. & Nasrallah, J. B. Generation of Self-Incompatible Arabidopsis thaliana by

635   Transfer of Two S Locus Genes from A. lyrata. *Science* **297,** 247–249 (2002).

636   25.   Hackett, R. M., Cadwallader, G. & Franklin, F. Functional Analysis of a Brassica oleracea SLR1

637   Gene Promoter. *Plant Physiol.* **112,** 1601–1607 (1996).

638   26.   Fobis-Loisy, I., Chambrier, P. & Gaude, T. Genetic transformation of Arabidopsis lyrata: Specific

639   expression of the green fluorescent protein (GFP) in pistil tissues. *Plant Cell Rep.* **26,** 745–753 (2007).

640   27.   Love, M. I., Huber, W. & Anders, S. Moderated estimation of fold change and dispersion for RNA-

641   seq data with DESeq2. *Genome Biol.* **15,** 550 (2014).

642   28.   Carr, D., Lewin-Koh, ported by N., Maechler, M. & Sarkar, contains copies of lattice functions

643   written by D. *hexbin: Hexagonal Binning Routines*. (2018).

644   29.   Dwyer, K. G., Lalonde, B. A., Nasrallah, J. B. & Nasrallah, M. E. Structure and expression of AtS1,

645   an Arabidopsis thaliana gene homologous to the S-locus related genes of Brassica. *Mol. Gen. Genet.*

646   *MGG* **231,** 442–448 (1992).

647   30.   Dwyer, K. G. *et al.* A superfamily of S locus-related sequences in Arabidopsis: diverse structures

648   and expression patterns. *Plant Cell* **6,** 1829–1843 (1994).

649   31.   Myers, C. *et al.* Calcium-dependent protein kinases regulate polarized tip growth in pollen tubes.

650   *Plant J.* **59,** 528–539 (2009).

651   32.   Honys, D. & Twell, D. Transcriptome analysis of haploid male gametophyte development in

652   Arabidopsis. *Genome Biol.* **5,** R85.1–R.85.13 (2004).

653   33.   Qin, Y. *et al.* Penetration of the stigma and style elicits a novel transcriptome in pollen tubes,

654   pointing to genes critical for growth in a pistil. *PLoS Genet.* **5,** (2009).

655   34.   Boavida, L. C., Borges, F., Becker, J. D. & Feijo, J. A. Whole Genome Analysis of Gene Expression

656   Reveals Coordinated Activation of Signaling and Metabolic Pathways during Pollen-Pistil Interactions

657   in Arabidopsis. *Plant Physiol.* **155,** 2066–2080 (2011).

658   35.   Osaka, M. *et al.* Cell type-specific transcriptome of brassicaceae stigmatic papilla cells from a

659   combination of laser microdissection and RNA sequencing. *Plant Cell Physiol.* **54,** 1894–1906 (2013).

660   36.   Ringnér, M. What is principal component analysis? *Nat. Biotechnol.* **26,** 303–304 (2008).

661   37.   Kanehisa, M., Furumichi, M., Tanabe, M., Sato, Y. & Morishima, K. KEGG: new perspectives on

662   genomes, pathways, diseases and drugs. *Nucleic Acids Res.* **45,** D353–D361 (2017).

663   38.   Bigeard, J., Colcombet, J. & Hirt, H. Signaling mechanisms in pattern-triggered immunity (PTI).

664   *Mol. Plant* **8,** 521–539 (2015).

665   39.   Obayashi, T., Aoki, Y., Tadaka, S., Kagaya, Y. & Kinoshita, K. ATTED-II in 2018: A Plant

666   Coexpression Database Based on Investigation of the Statistical Property of the Mutual Rank Index.

667   *Plant Cell Physiol.* **59,** e3–e3 (2018).

668   40.   Li, X., Lassner, M. & Zhang, Y. Deleteagene: A fast neutron deletion mutagenesis-based gene

669   knockout system for plants. *Comp. Funct. Genomics* **3,** 158–160 (2002).

670   41.   Miles, G. P., Samuel, M. A., Zhang, Y. & Ellis, B. E. RNA interference-based (RNAi) suppression of

671   AtMPK6, an Arabidopsis mitogen-activated protein kinase, results in hypersensitivity to ozone and

672   misregulation of AtMPK3. *Environ. Pollut.* **138,** 230–237 (2005).

673   42.   Genenncher, B. *et al.* Nucleoporin-Regulated MAP Kinase Signaling in Immunity to a

674   Necrotrophic Fungal Pathogen. *Plant Physiol.* **172,** 1293–1305 (2016).

675   43.   Dickinson, H. Simply a social disease? *Nature* **367,** 517–518 (1994).

676   44.   Nasrallah, J. B. Recognition and rejection of self in plant self-incompatibility: Comparisons to

677   animal histocompatibility. *Trends Immunol.* **26,** 412–418 (2005).

678   45.   Mondragon, M., John-Arputharaj, A., Pallmann, M. & Dresselhaus, T. Similarities between

679   reproductive and immune pistil transcriptomes of Arabidopsis species. *Plant Physiol.* pp.00390.2017

680   (2017). doi:10.1104/pp.17.00390

681   46.   Tung, C. *et al.* Genome-Wide Identification of Genes Expressed in Arabidopsis Pistils Specifically

682   along the Path of Pollen Tube Growth 1 [w]. *Plant Physiol.* **138,** 1–13 (2005).

683   47.   Sanati Nezhad, A. & Geitmann, A. The cellular mechanics of an invasive lifestyle. *J. Exp. Bot.* **64,**

684   4709–4728 (2013).

685   48.   Marsollier, A.-C. & Ingram, G. Getting physical: invasive growth events during plant

686   development. *Curr. Opin. Plant Biol.* **46,** 8–17 (2018).

687   49.   Velázquez, E. *et al.* The Coexistence of Symbiosis and Pathogenicity-Determining Genes in

688   Rhizobium rhizogenes Strains Enables Them to Induce Nodules and Tumors or Hairy Roots in Plants.

689   *Mol. Plant. Microbe Interact.* **18,** 1325–1332 (2005).

690   50.   Chen, T. *et al.* Interplay of pathogen-induced defense responses and symbiotic establishment in

691   Medicago truncatula. *Front. Microbiol.* **8,** 1–13 (2017).

692   51.   Hamilton, E. S. *et al.* Mechanosensitive channel MSL8 regulates osmotic forces during pollen

693   hydration and germination. *Science* **350,** 438–441 (2015).

694   52.   Mecchia, M. A. *et al.* RALF4/19 peptides interact with LRX proteins to control pollen tube growth

695   in Arabidopsis. *Science* **358,** 1600–1603 (2017).

696   53.   Ge, Z. *et al.* Arabidopsis pollen tube integrity and sperm release are regulated by RALF-mediated

697   signaling. *Science* **358,** 1596–1600 (2017).

698   54.   Kohorn, B. D. & Kohorn, S. L. The cell wall-associated kinases, WAKs, as pectin receptors. *Front.*

699   *Plant Sci.* **3,** (2012).

700   55.   Kohorn, B. D. The state of cell wall pectin monitored by wall associated kinases: A model. *Plant*

701   *Signal. Behav.* **10,** e1035854 (2015).

702   56.   Park, A. R. *et al.* Interaction of the Arabidopsis Receptor Protein Kinase Wak1 with a Glycine-rich

703   Protein, AtGRP-3. *J. Biol. Chem.* **276,** 26688–26693 (2001).

704   57.   Karimi, M., Inzé, D. & Depicker, A. GATEWAY™ vectors for Agrobacterium-mediated plant

705   transformation. *Trends Plant Sci.* **7,** 193–195 (2002).

706   58.   Durand, E. *et al.* Dominance hierarchy arising from the evolution of a complex small RNA

707   regulatory network. *Science* **346,** 1200–1205 (2014).

708   59.   Logemann, E., Birkenbihl, R. P., Ülker, B. & Somssich, I. E. An improved method for preparing

709   Agrobacterium cells that simplifies the Arabidopsis transformation protocol. *Plant Methods* **2,** 16

710   (2006).

711   60.   Smyth, D. R., Bowman, J. L. & Meyerowitz, E. M. Early flower development in Arabidopsis. *Plant*

712   *Cell* **2,** 755–767 (1990).

713   61.   Kitashiba, H., Liu, P., Nishio, T., Nasrallah, J. B. & Nasrallah, M. E. Functional test of Brassica self-

714   incompatibility modifiers in Arabidopsis thaliana. *Proc. Natl. Acad. Sci.* **108,** 18173–18178 (2011).

715   62.   Verger, S., Chabout, S., Gineau, E. & Mouille, G. Cell adhesion in plants is under the control of

716   putative O-fucosyltransferases. *Development* **143,** 2536–2540 (2016).

717   63.   Li, H. & Durbin, R. Fast and accurate short read alignment with Burrows–Wheeler transform.

718   *Bioinformatics* **25,** 1754–1760 (2009).

719   64.   McKenna, A. *et al.* The Genome Analysis Toolkit: A MapReduce framework for analyzing next-

720   generation DNA sequencing data. *Genome Res.* **20,** 1297–1303 (2010).

721   65.   DePristo, M. A. *et al.* A framework for variation discovery and genotyping using next-generation

722   DNA sequencing data. *Nat. Genet.* **43,** 491–498 (2011).

723   66.   Auwera, G. A. V. der *et al.* From FastQ Data to High-Confidence Variant Calls: The Genome

724   Analysis Toolkit Best Practices Pipeline. *Curr. Protoc. Bioinforma.* **43,** 11.10.1–11.10.33 (2013).

725   67.   Otto, T. D., Dillon, G. P., Degrave, W. S. & Berriman, M. RATT: Rapid Annotation Transfer Tool.

726   *Nucleic Acids Res.* **39,** e57–e57 (2011).

727   68.   Rice, P., Longden, I. & Bleasby, A. EMBOSS: The European Molecular Biology Open Software

728   Suite. *Trends Genet.* **16,** 276–277 (2000).

729   69.   Hamada, M., Ono, Y., Asai, K., Frith, M. C. & Hancock, J. Training alignment parameters for

730   arbitrary sequencers with LAST-TRAIN. *Bioinformatics* **33,** 926–928 (2017).

731   70.   Langmead, B., Trapnell, C., Pop, M. & Salzberg, S. L. Ultrafast and memory-efficient alignment of

732   short DNA sequences to the human genome. *Genome Biol.* **10,** R25 (2009).

733   71.   Mi, H., Muruganujan, A. & Thomas, P. D. PANTHER in 2013: modeling the evolution of gene

734   function, and other gene attributes, in the context of phylogenetic trees. *Nucleic Acids Res.* **41,** D377–

735   D386 (2013).

736   72.   Thomas, P. D. *et al.* PANTHER: A Library of Protein Families and Subfamilies Indexed by Function.

737   *Genome Res.* **13,** 2129–2141 (2003).

738

748 **Author Contributions:** CK, JJ, MDR developed the data analysis pipeline and performed the

749 bioinformatics analyses. AL, JL supported the bioinformatics analyses. AL helped with

750 interpretation of the transcriptomic data. CK is responsible for all experiments and analysis

751 performed in the study except described below. FR produced and characterized Col-0/*SRK14* and

752 C24/*SCR14* lines. CK and LR performed the image acquisition by scanning electron microscope.

753 CK, LR, FR, IFL harvested plant materials and extracted RNA. CK, TG, IFL designed the study

754 and CK, JJ, TG, IFL wrote the manuscript. All the authors contributed to the discussion.

755

Figure legends:

757 **Fig. 1 | SNP-based RNA-seq analysis. a**, Time course of sample collection. Flowers of Col-
758 0/*SRK14* were emasculated 16h - 20h before pollination with compatible (C24) or incompatible
759 (C24/*SCR14*) pollen grains, respectively. Stigmas were harvested just before the stigma
760 (dashed line) 0, 10, 60 min after compatible (C0, C10, C60) or incompatible (I10, I60) pollination
761 for RNA extraction. Typical scanning electron microscope images for compatible (Col-0 /*SRK14*
762 x C24) and incompatible (Col-0 /*SRK14* x C24/*SCR14*) reaction observed 60 min after
763 pollination. Scale bar = 20 μm. **b**, Three steps of a SNP-based data analysis pipeline. **c**, Number
764 of predicted mRNAs derived from the reference sequence produced at the second step in b.
765 Around 80 % of coding regions have SNPs between Col-0/SRK14 and C24. **d**, Number and ratio
766 of estimated read counts for Col-0/*SRK14* and C24 at C0 computed by ASE-TIGAR at the third
767 step in b. Reads estimated to the stigma or pollen include reads assigned to the genes without
768 using SNPs. **e**, Hexibin plot of nFPKM for Col-0/*SRK14* and C24 at C0. nFPKM(stigma) of genes
769 without SNPs were plotted outside.

771 **Fig. 2 | Validation of the SNP-based analysis. a**, Number of stigma or pollen (preferentially /
772 specifically) -expressed genes at C0 selected by nFPKM (Supplementary Table 5). **b**, RT-PCR
773 and sequence analysis of stigma or pollen specifically-expressed genes at C0. The genes are
774 selected among the 20 specifically-expressed genes and the rank of the genes according to the
775 expression level are presented. RNA was extracted from pollinated stigmas at C0 then we
776 analysed their SNP-information by RT-PCR and sequencing. SNP number corresponds to the
777 number of SNPs present in the sequenced regions. **c**, Heat map of Pearson's correlation
778 coefficient between the stigma/pollen transcripts from the SNP-based analysis and the
779 previously published transcripts. **d**, Top ten gene enrichment categories of stigma or pollen
780 preferentially-expressed genes at C0 according to the GO term on biological processes.
781 Enrichment analysis was performed with the one thousand top expressed genes in stigma (left)
782 or pollen (right) among the list, respectively. Only top 10 first enrichment categories are shown.
783 Selection criteria for genes analysed in **b** (sex-specific), and **d** (sex-preferential), are described
784 in the manuscript.

786 **Fig. 3 | Gene expression dynamics after pollination. a**, PCA of stigma (left) and pollen (right)
787 transcripts. Biological replicates of all the conditions were analysed. **b**, Venn diagrams showing
788 the number of up-regulated (FC > 2) genes in stigma (left) and pollen (right), after compatible
789 (green and violet) or incompatible (grey) pollinations. **c**, Gene enrichment categories of up-

790 regulated genes after compatible pollination in stigma according to GO term on biological
791 processes. Only genes specifically induced after compatible reaction (b, left; 158+163+623)
792 were analysed. Only top 20 enrichment categories are shown.
793
794 **Fig. 4 | Induced genes in PTI pathways after pollination in stigma.**
795 KEGG pathway mapping applied for the genes exclusively up-regulated after compatible
796 pollination (Fig.3 b, left; 158+163+623) and incompatible pollination (Fig.3 b, left; 4+0+104),
797 respectively. Green colored genes were identified from the compatible gene set and grey were
798 from the incompatible set. Up-regulated gene in our analysis assigned to *BAK1*/*BKK1* was
799 *SERK4*, and to *MKK1/2* was *MKK6* (see Fig. 5 and Supplementary Table 10).
800
801 **Fig. 5 | Induced pathways in stigma after compatible pollination.** Genes in green boxes with
802 solid line were with SNPs and up-regulated (FC > 2) at 10 min and 60 min (light green), or only
803 at 60 min (green), genes in orange boxes with dashed line were without SNPs and up-regulated
804 (FC > 2) at 10 min and 60 min (orange), or only at 60 min (dark orange). Genes written in bold
805 were expressed at C0; nFPKM(stigma) > 1. The pathway map from KEGG database was
806 modified with the information from Bigeard et al. 2015.
807
808 **Fig.6 | Activation of a MPK3-dependent pathway after compatible pollination.**
809 Immunoblotting assays after compatible pollination with *mpk3* mutant line. Pollination between
810 Col-0 x Col-0, *mpk3* x *mpk3*, Col-0 x *mpk3*, and *mpk3* x Col-0 were performed. Protein was
811 extracted from pollinated stigmas at C0 and C60 then analysed. Anti-MPK3 antibody was used
812 for **a**, and anti-phospho-p44/42 MPK antibody was used for **c**. The shown western blots are
813 representative of three independent biological replicates. All of them showed similar results. **b**.,
814 **d**. Semi-quantification of the band intensity (b for a, d for c). Green, violet and grey bars indicate
815 signals from stigma side, from pollen side, and from both sides, respectively. Error bars indicate
816 standard error of the mean, ** indicates non-specific signal, *** indicates non-specific signal or
817 signals from other MPK proteins.
818
819 **Fig.7 | *mpk3* stigma changes the width of pollen tube contact sites. a**, Pollen tube contact
820 sites on Col-0 (left) or *mpk3* (right) papilla cells observed by SEM 60 min after pollination. One
821 stigma papilla is artificially colorized in green and one pollen grain and its tube in violet,
822 respectively. Scale bar = 10 μm. Double-arrows indicate the width of pollen tube contact site
823 analysed in b. **b**, Width of the pollen tube contact site for each pollination type presented in a.
824 Observations were performed three different days; n is the total number of contact sites
825 measured on 16 Col-0 and 25 *mpk3* stigmas. Orange points in the boxes are averages of each
826 day.*** indicates p-value < 0.01.
827
828 **Fig.8 | Stigma-pollen interaction involves MPK3-dependent pathway.** Schematic model for
829 stigma-pollen interaction. i, Signals at the contact site between pollen tube and papilla cell. ii,
830 Signal transduction involving MPK3 pathways. iii, Gene expression change. iv, Protein
831 activations without transcriptomic change v, Stigma cell wall reorganization. vi, Effect on pollen
832 tube by stigma surface property.
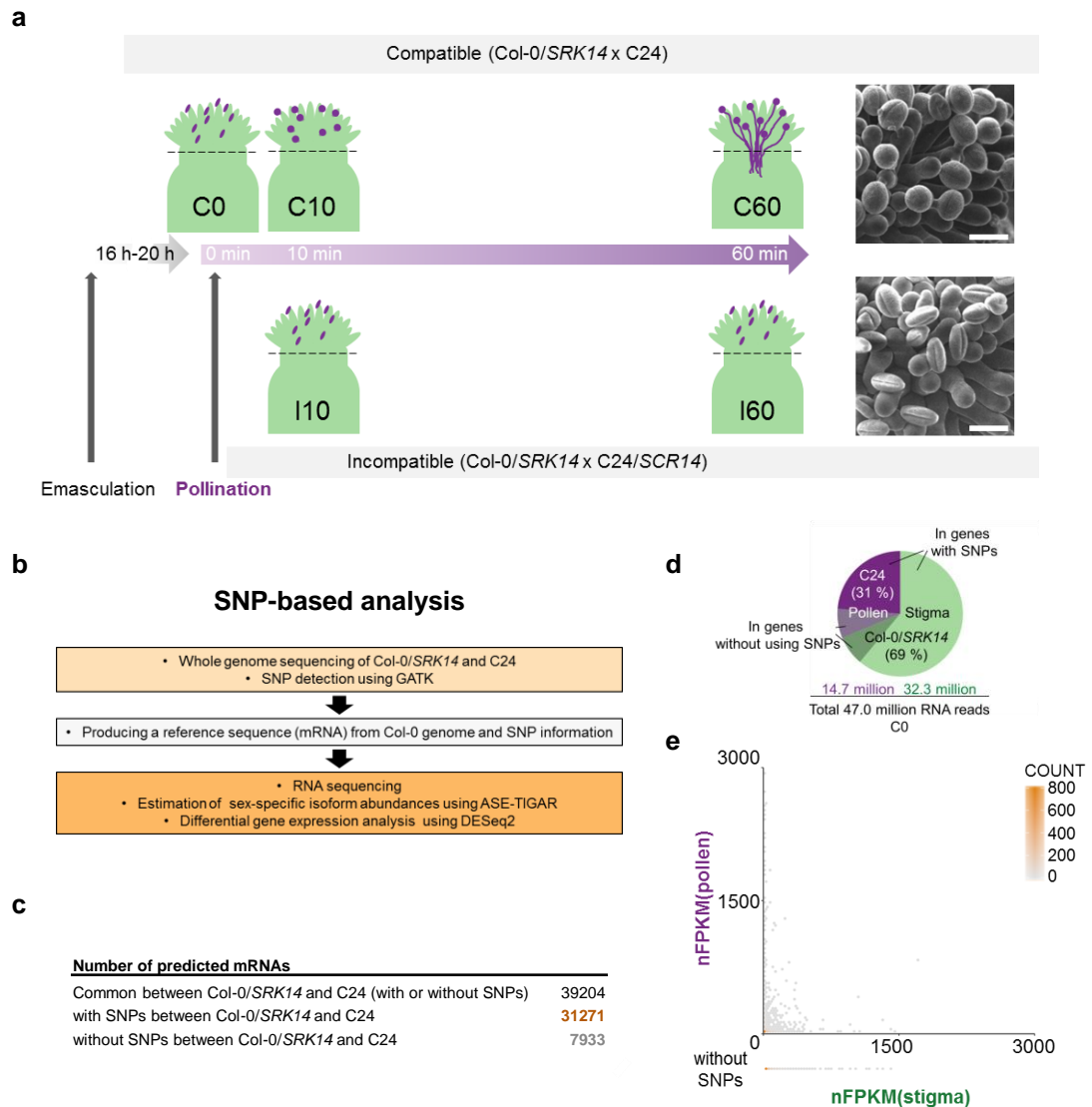833

Additional information:

835 Supplementary Fig. 1
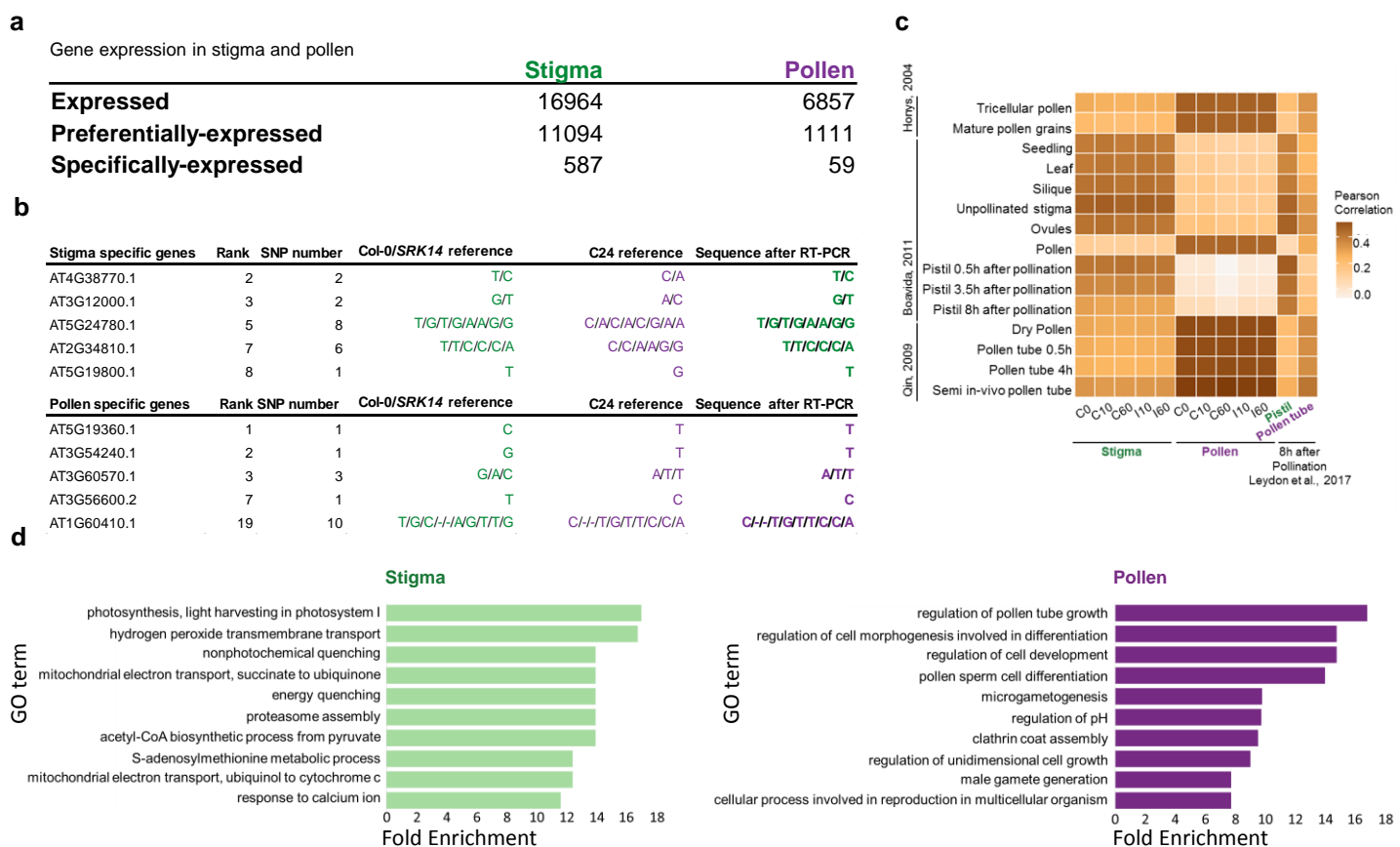
836 Supplementary Fig. 2
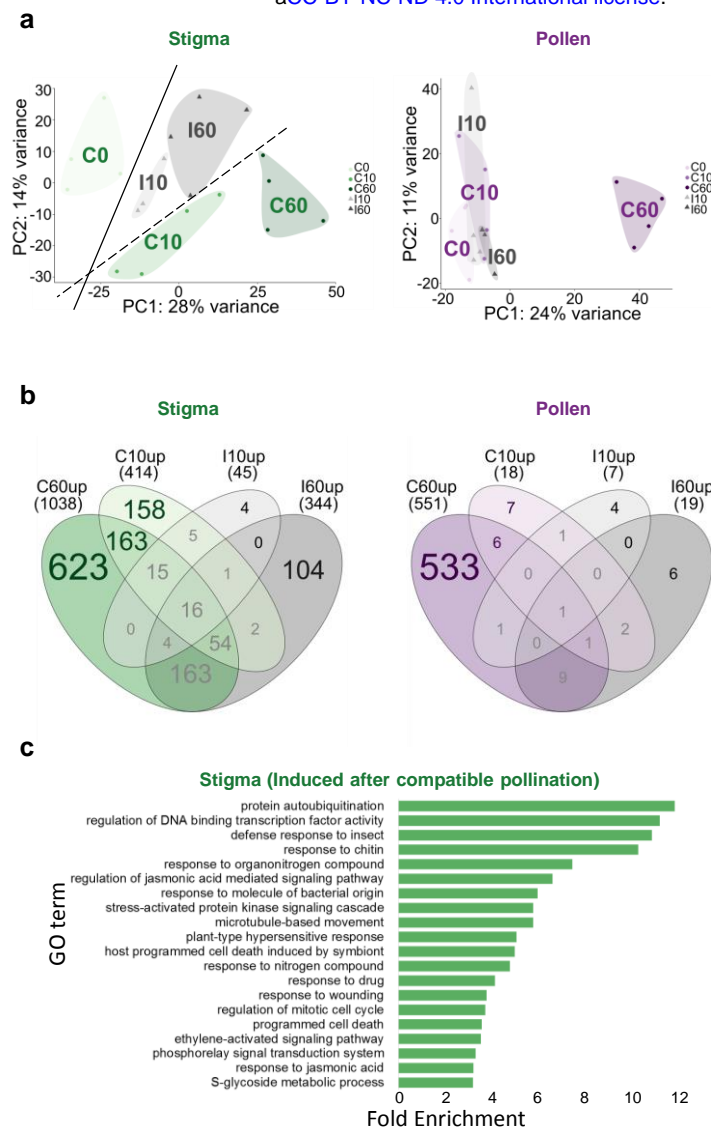
837   Supplementary Fig. 3

838   Supplementary Fig. 4

839   Supplementary Fig. 5

840   Supplementary Fig. 6

841   Supplementary Table. 1

842   Supplementary Table. 2

843   Supplementary Table. 3

844   Supplementary Table. 4

845   Supplementary Table. 5

846   Supplementary Table. 6

847   Supplementary Table. 7

848   Supplementary Table. 8

849   Supplementary Table. 9

850   Supplementary Table. 10

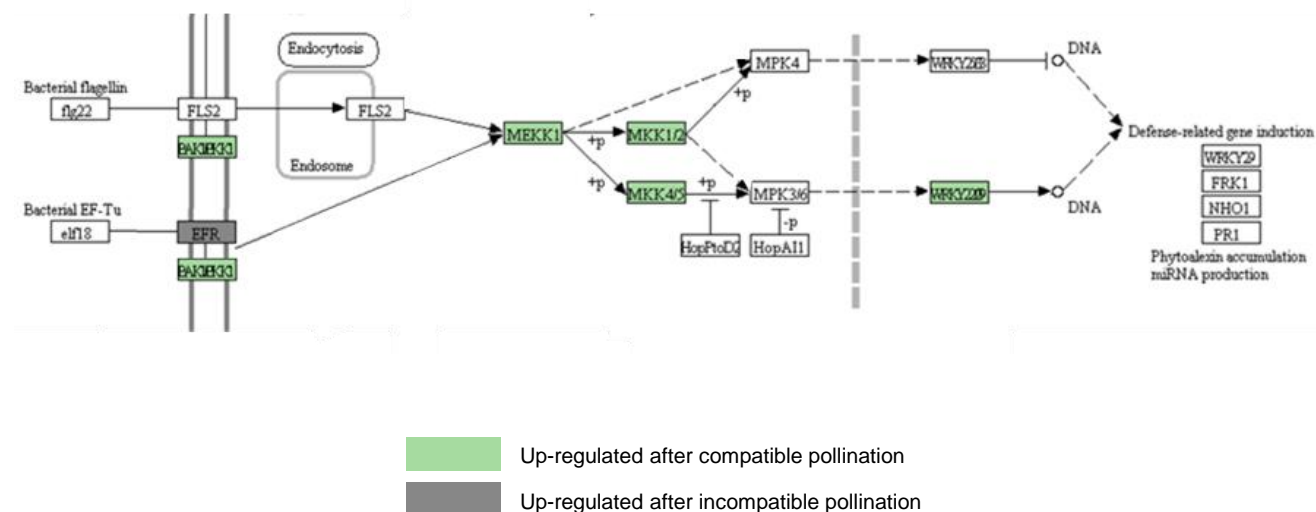851   Supplementary Table. 11

852

Fig. 1 | SNP-based RNA-seq analysis. a, Time course of sample collection. Flowers of Col-0/*SRK14* were emasculated 16h - 20h before pollination with compatible (C24) or incompatible (C24/*SCR14*) pollen grains, respectively. Stigmas were harvested just before the stigma (dashed line) 0, 10, 60 min after compatible (C0, C10, C60) or incompatible (I10, I60) pollination for RNA extraction. Typical scanning electron microscope images for compatible (Col-0 /*SRK14* x C24) and incompatible (Col-0 /*SRK14* x C24/*SCR14*) reaction observed 60 min after pollination. Scale bar = 20 µm. **b**, Three steps of a SNP-based data analysis pipeline. **c**, Number of predicted mRNAs derived from the reference sequence produced at the second step in b. Around 80 % of coding regions have SNPs between Col-0/SRK14 and C24. **d**, Number and ratio of estimated read counts for Col-0/*SRK14* and C24 at C0 computed by ASE-TIGAR at the third step in b. Reads estimated to the stigma or pollen include reads assigned to the genes without using SNPs. **e**, Hexibin plot of nFPKM for Col-0/*SRK14* and C24 at C0. nFPKM(stigma) of genes without SNPs were plotted outside.

a

Gene expression in stigma and pollen

	Stigma	Pollen
Expressed	16964	6857
Preferentially-expressed	11094	1111
Specifically-expressed	587	59

b

Stigma specific genes	Rank	SNP number	Col-0/*SRK14* reference	C24 reference	Sequence after RT-PCR
AT4G38770.1	2	2	T/C	C/A	T/C
AT3G12000.1	3	2	G/T	A/C	G/T
AT5G24780.1	5	8	T/G/T/G/A/A/G/G	C/A/C/A/C/G/A/A	T/G/T/G/A/A/G/G
AT2G34810.1	7	6	T/T/C/C/C/A	C/C/A/A/G/G	T/T/C/C/C/A
AT5G19800.1	8	1	T	G	T

Pollen specific genes	Rank	SNP number	Col-0/*SRK14* reference	C24 reference	Sequence after RT-PCR
AT5G19360.1	1	1	C	T	T
AT3G54240.1	2	1	G	T	T
AT3G60570.1	3	3	G/A/C	A/T/T	A/T/T
AT3G56600.2	7	1	T	C	C
AT1G60410.1	19	10	T/G/C/-/-/A/G/T/T/G	C/-/-/T/G/T/T/C/C/A	C/-/-/T/G/T/T/C/C/A

c

d

Fig. 2 | Validation of the SNP-based analysis. a, Number of stigma or pollen (preferentially / specifically) -expressed genes at C0 selected by nFPKM (Supplementary Table 5). **b**, RT-PCR and sequence analysis of stigma or pollen specifically-expressed genes at C0. The genes are selected among the 20 specifically-expressed genes and the rank of the genes according to the expression level are presented. RNA was extracted from pollinated stigmas at C0 then we analysed their SNP-information by RT-PCR and sequencing. SNP number corresponds to the number of SNPs present in the sequenced regions. **c**, Heat map of Pearson's correlation coefficient between the stigma/pollen transcripts from the SNP-based analysis and the previously published transcripts. **d**, Top ten gene enrichment categories of stigma or pollen preferentially-expressed genes at C0 according to the GO term on biological processes. Enrichment analysis was performed with the one thousand top expressed genes in stigma (left) or pollen (right) among the list, respectively. Only top 10 first enrichment categories are shown. Selection criteria for genes analysed in **b** (sex-specific), and **d** (sex-preferential), are described in the manuscript.
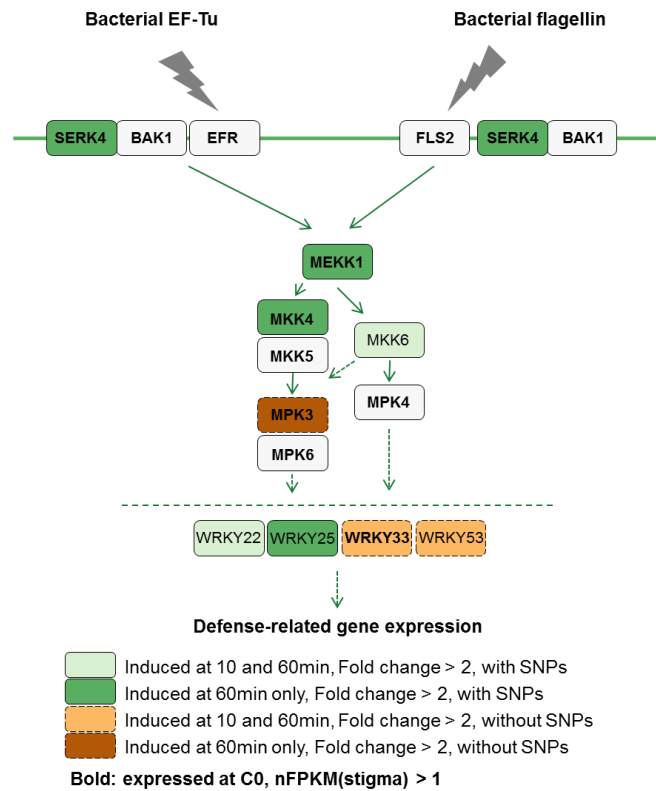
Fig. 3 | Gene expression dynamics after pollination. a, PCA of stigma (left) and pollen (right) transcripts. Biological replicates of all the conditions were analysed. **b**, Venn diagrams showing the number of up-regulated (FC > 2) genes in stigma (left) and pollen (right), after compatible (green and violet) or incompatible (grey) pollinations. **c**, Gene enrichment categories of up-regulated genes after compatible pollination in stigma according to GO term on biological processes. Only genes specifically induced after compatible reaction (b, left; 158+163+623) were analysed. Only top 20 enrichment categories are shown.
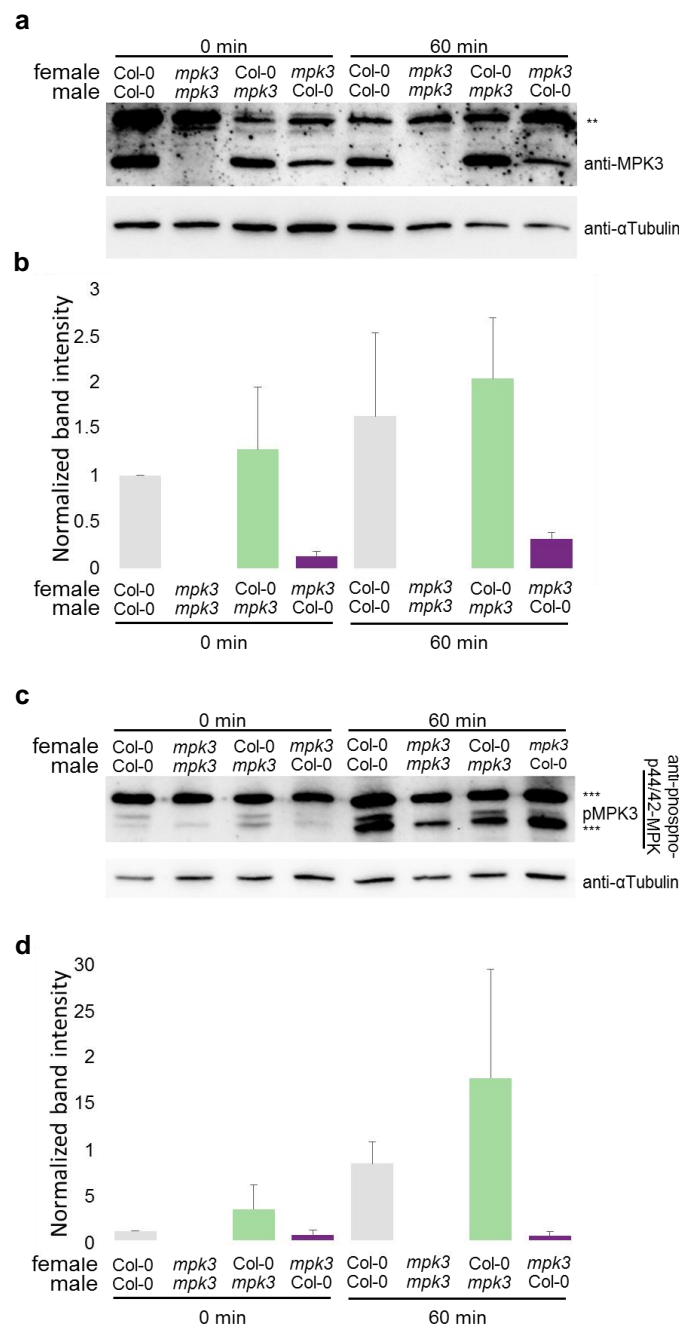
Up-regulated after compatible pollination

Up-regulated after incompatible pollination

Fig. 4 | Induced genes in PTI pathways after pollination in stigma.

KEGG pathway mapping applied for the genes exclusively up-regulated after compatible pollination (Fig.3 b, left; 158+163+623) and incompatible pollination (Fig.3 b, left; 4+0+104), respectively. Green colored genes were identified from the compatible gene set and grey were from the incompatible set. Up-regulated gene in our analysis assigned to *BAK1/BKK1* was *SERK4*, and to *MKK1/2* was *MKK6* (see Fig. 5 and Supplementary Table 10).
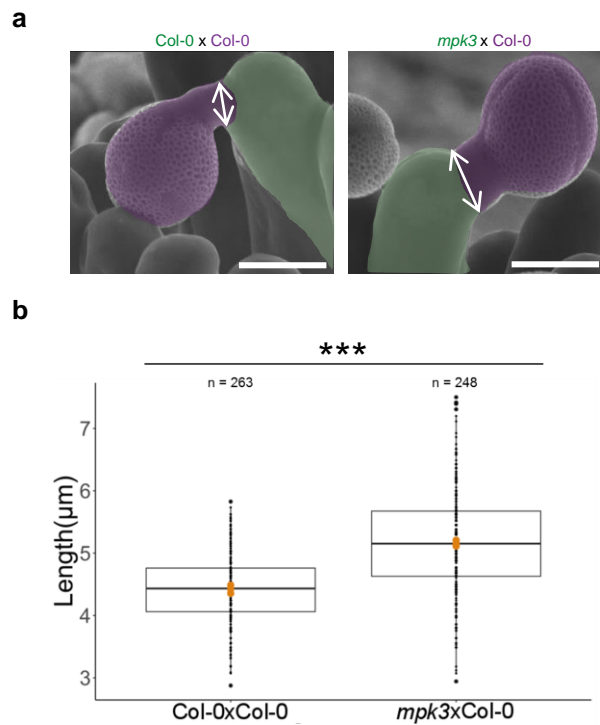
Fig. 5 | Induced pathways in stigma after compatible pollination. Genes in green boxes with solid line were with SNPs and up-regulated (FC > 2) at 10 min and 60 min (light green), or only at 60 min (green), genes in orange boxes with dashed line were without SNPs and up-regulated (FC > 2) at 10 min and 60 min (orange), or only at 60 min (dark orange). Genes written in bold were expressed at C0; nFPKM(stigma) > 1. The pathway map from KEGG database was modified with the information from Bigeard et al. 2015.
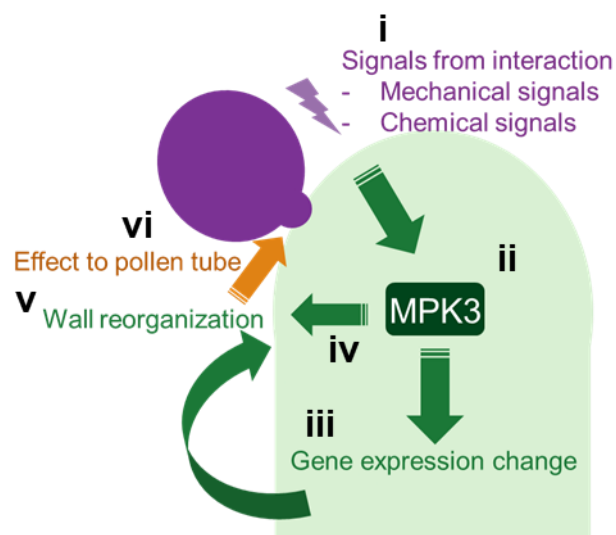
Fig.6 | Activation of a MPK3-dependent pathway after compatible pollination. Immunoblotting assays after compatible pollination with *mpk3* mutant line. Pollination between Col-0 x Col-0, *mpk3* x *mpk3*, Col-0 x *mpk3*, and *mpk3* x Col-0 were performed. Protein was extracted from pollinated stigmas at C0 and C60 then analysed. Anti-MPK3 antibody was used for **a**, and anti-phospho-p44/42 MPK antibody was used for **c**. The shown western blots are representative of three independent biological replicates. All of them showed similar results. **b**., **d**. Semi-quantification of the band intensity (b for a, d for c). Green, violet and grey bars indicate signals from stigma side, from pollen side, and from both sides, respectively. Error bars indicate standard error of the mean, ** indicates non-specific signal, *** indicates non-specific signal or signals from other MPK proteins.

Fig.7 | *mpk3* stigma changes the width of pollen tube contact sites. a, Pollen tube contact sites on Col-0 (left) or *mpk3* (right) papilla cells observed by SEM 60 min after pollination. One stigma papilla is artificially colorized in green and one pollen grain and its tube in violet, respectively. Scale bar = 10 μm. Double-arrows indicate the width of pollen tube contact site analysed in b. **b**, Width of the pollen tube contact site for each pollination type presented in a. Observations were performed three different days; n is the total number of contact sites measured on 16 Col-0 and 25 *mpk3* stigmas. Orange points in the boxes are averages of each day.*** indicates p-value < 0.01.

Fig.8 | Stigma-pollen interaction involves MPK3-dependent pathway. Schematic model for stigma-pollen interaction. i, Signals at the contact site between pollen tube and papilla cell. ii, Signal transduction involving MPK3 pathways. iii, Gene expression change. iv, Protein activations without transcriptomic change v, Stigma cell wall reorganization. vi, Effect on pollen tube by stigma surface property.